Chemical Engineering Science 322 (2026) 122977

Contents lists available at ScienceDirect

Chemical Engineering Science

journal homepage: www.elsevier.com/locate/ces

The hydrodynamics of pseudo-2D and 3D bubbling fluidized beds: A magnetic resonance imaging study

Hannah S. Rennebaum, Daniel L. Brummerloh, Stefan Benders, Alexander Penn *

Institute of Process Imaging, Hamburg University of Technology, Hamburg, Germany

ARTICLE INFO

Keywords:
Bubbling fluidized beds
Pseudo-two-dimensional fluidized beds
Magnetic resonance imaging
Wall effects
Bubble dynamics
Particle velocity

ABSTRACT

Real-time magnetic resonance imaging (MRI) was used to compare the hydrodynamics of three-dimensional (3D) and pseudo-two-dimensional (2D) gas-solid fluidized beds of various wall separation distances by measuring the particle distribution and velocity. Five different superficial gas velocities from one to two times the minimum fluidization velocity and four pseudo-2D bed thicknesses between 15 and 50 mm were investigated. A neural network model was used to segment gas bubbles, revealing that thinner beds homogenize the radial bubble distribution and reduce the average equivalent bubble diameter compared to 3D beds. Furthermore, pseudo-2D beds showed lower bubble rise and average particle velocities. Based on the findings, an existing correlation for predicting bubble rise velocity is extended by incorporating an additional term that accounts for the influence of bed thickness. The minimum fluidization velocity and the expansion ratio increases as the bed thickness decreases. Yet, the shape of the bubbles in pseudo-2D fluidized bed remains unaffected when compared to 3D fluidized beds. Pseudo-2D fluidized beds with a smaller thickness, typically employed in optical experiments, exhibited the greatest deviation in hydrodynamics compared to 3D fluidized beds.

1. Introduction

Gas-solid fluidized beds are widely used in industrial applications because of their high mass and heat transfer rates compared to conventional fixed-bed systems (Crowe, 2006). Due to their complex behavior, the hydrodynamics of fluidized beds have been continuously investigated since their introduction more than a century ago (Winkler, 1926). Traditional methods such as capacitance (Wiesendorf and Werther, 2000), electrostatic (He et al., 2015), and optical (Rüdisüli et al., 2012; Li et al., 2012b; Taofeeq et al., 2018; Varghese et al., 2021) probes within the bulk phase have been used to understand and predict the hydrodynamics in three-dimensional (3D) fluidized beds. Optical fiber probes have been used to investigate the bubble size distribution and rise velocity (Rüdisüli et al., 2012; Li et al., 2012b), as well as the velocities of the solid phase and the gas holdup (Taofeeq et al., 2018; Varghese et al., 2021). Although optical fiber probes are intrusive, Maurer et al. have shown that for single rising bubbles at minimum fluidization velocity, the introduced probes have minimal impact on bubble size, bubble shape, and bubble rise velocity (Maurer et al., 2015). Yet, probes are limited to local measurements and do not offer a comprehensive view of the entire fluidized bed. To capture the overall hydrodynamics, pseudo-two-dimensional (2D) fluidized bed setups are often used, simplifying the geometry for enhanced optical accessibility. These setups, combined with digital image analysis (DIA), have been used to study the impact of various parameters, such as particle size (Zhu et al., 2023) and shape (Mahajan et al., 2018), vibration (Cano-Pleite et al., 2016; Guo et al., 2021), and membranes with permeating gas (de Jong et al., 2013), on the hydrodynamics of the bed. Advanced techniques such as particle image velocimetry (PIV) and particle tracking velocimetry (PTV) (Hagemeier et al., 2015) further enable the calculation of particle velocity fields (Laverman et al., 2008; Hernández-Jiménez et al., 2011). Due to the simplification from 3D to a pseudo-2D fluidized beds, it remains uncertain to what extent the findings can be reliably extrapolated to 3D systems. For comprehensive and non-invasive measurements of fluidized beds, tomographic techniques such as X-ray imaging (Errigo et al., 2023) and magnetic resonance imaging (MRI) (Penn et al., 2018, 2019; Boyce et al., 2019b; Rennebaum et al., 2024, 2025) can be used. The limited temporal resolution of MRI can be increased sufficiently by combining parallel imaging using tailored radio frequency (RF) detection arrays and time-efficient single-shot pulse sequences (Penn et al., 2017) to enable 2D real-time measurements of the hydrodynamics of fluidized beds. In the past, this was used to investigate the impact of internals (Penn et al., 2019; Rennebaum et al., 2024, 2025) and small amount of injected water (Boyce et al., 2019a) on the hydrodynamics of fluidized beds. Compared to other measurement techniques for solid-gas systems, the particles used for MRI have to contain NMR visible

* Corresponding author.
E-mail address: alexander.penn@tuhh.de (A. Penn).

https://doi.org/10.1016/j.ces.2025.122977
Received 23 September 2025; Received in revised form 5 November 2025; Accepted 11 November 2025
Available online 20 November 2025

materials, such as water or oil. Combined with its higher experimental complexity, this requirement makes MRI less accessible than traditional probes or pseudo-2D fluidized beds. This complexity limits their use for online monitoring, which is typically achieved with simpler pressure and optical probes.

Comparing the different investigation methods raises the question about the extent to which data obtained from pseudo-2D fluidized beds can be extrapolated to 3D systems, potentially diminishing the need for more complex tomographic techniques. Addressing this question is particularly relevant given that optical measurements in pseudo-2D beds offer significantly higher spatial and temporal resolution than conventional techniques typically allow in 3D fluidized beds (Sánchez-Delgado et al., 2011). If the findings from pseudo-2D systems prove transferable, the need for more complex tomographic approaches could be reduced. However, there is evidence that gas bubble behavior differs between the two configurations, as bubble growth in pseudo-2D beds is constrained in one dimension, potentially affecting flow dynamics (Geldart, 1970).

Several experimental and simulation studies have explored how the simplified geometry of pseudo-2D fluidized beds alters their hydrodynamics compared to 3D beds. Li et al. used CFD-DEM simulations to study the effect of bed thickness on static bed height, bubble behavior, and solid velocities (Li et al., 2012a). They found that solid velocities exhibit significant 3D behavior for bed thicknesses up from $t_{bed} > 40d_p$. In contrast, for the bed thickness between $10d_p$ and $20d_p$, the velocities indicate the 2D flow behavior and in between ($20d_p < t_{bed} < 40d_p$), they identified a transition zone. In addition to simulation-based approaches, experimental studies have investigated parameters such as the minimum fluidization velocity and the bubble rise velocity. Saxena et al. found that the minimum fluidization velocity within pseudo-2D fluidized beds, $U_{mf,2D}$, increases as the thickness of the bed decreases (Saxena and Vadivel, 1988), due to the restrictive influence of the walls on the movement of the particles. They proposed a correlation to calculate the minimum fluidization velocity based on the diameter of the particle, d_p [mm] and the bed thickness, t_{bed} [mm] (Eq. (1)).

$$U_{mf,2D} = 3.513 - 3.22\left(\frac{t_{bed}}{1000}\right) + 0.428\ln\left(\frac{d_p}{1000}\right) \quad (1)$$

Sánchez-Delgado et al. described a correlation between the minimum fluidization velocity in pseudo-2D and 3D fluidized beds, introducing a and b as fitting parameters:

$$\frac{U_{mf,2D}}{U_{mf,3D}} = \exp\left(a\left(\frac{d_p}{t_{bed}}\right)^b\right) \quad (2)$$

Once fluidized beds exceed a critical bed thickness with $t_{bed} > 100d_p$, wall effects on the minimum fluidization velocity have reported to become negligible (Sánchez-Delgado et al., 2011). Unlike 3D fluidized beds, the minimum fluidization velocity in pseudo-2D fluidized beds increases with greater filling heights (Geldart and Cranfield, 1972; Ramos Caicedo et al., 2002). Beyond the minimum fluidization velocity, Geldart determined the average diameter of bursting bubbles at the surface of pseudo-2D and 3D fluidized beds, observing larger bubbles within the 3D fluidized beds (Geldart, 1970). Glicksman and McAndrews used fiber optic probes to show that bubbles of the same diameter rise faster in a 3D than in a pseudo-2D fluidized bed (Glicksman and McAndrews, 1985). Hernández-Jiménez et al. (2013) determined the particle-wall interaction coefficient in a pseudo-2D fluidized bed using pressure signals together with solid distribution data from optical measurements, and found higher coefficients for larger particles. These studies strongly suggest that the hydrodynamic behavior of pseudo-2D fluidized beds differs significantly from that of 3D fluidized beds, primarily due to the influence of wall effects. Yet, previous experimental studies have relied exclusively on probes placed within the fluidized bed or optical measurements from the outside of the bed, which limited the ability to obtain a comprehensive view of the system and left the influence of bed thicknesses insufficiently understood. In addition, the effect of pseudo-2D and 3D fluidized beds on the particle velocity remains unclear.

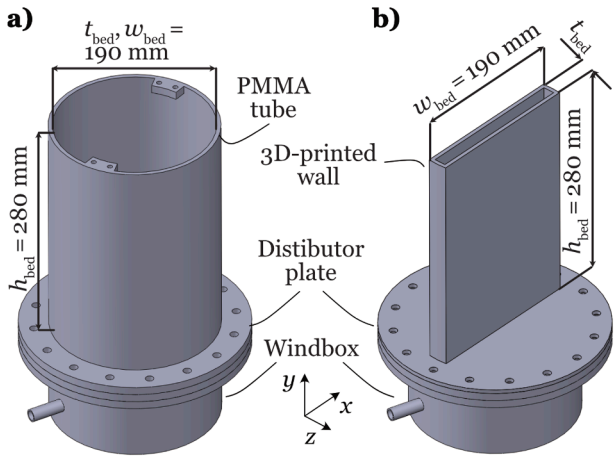

Fig. 1. Schematics of the (a) 3D fluidized bed model and (b) the pseudo-2D fluidized bed model. Pseudo-2D fluidized bed with bed thickness of 15, 20, 30, and 50 mm were investigated. MRI measurements of the particle density and velocity were taken in vertical orientation.

This study employs MRI to compare the hydrodynamics within a pseudo-2D fluidized bed with varying bed thicknesses between 15 and 50 mm with those of a 3D fluidized bed with a diameter of 190 mm. Unlike previous studies, the application of a tomographic technique enables non-intrusive measurements of hydrodynamics in pseudo-2D beds and allows direct comparison with equivalent 3D systems. In addition to identifying potential differences, a central objective was to determine whether there is a critical bed thickness in pseudo-2D systems at which the hydrodynamic behavior closely approximates that of a 3D fluidized bed. Local particle concentration and velocity were measured to determine the equivalent bubble diameter, bubble rise velocity, aspect ratio, bed expansion, bubble accessibility, and the average in-plane particle velocity.

2. Methods

2.1. Fluidized bed

The gas-solid fluidized bed model was made from a Poly(methyl methacrylate) (PMMA) tube with an inner diameter of 190 mm and a height of 280 mm (Fig. 1a). The pseudo-2D fluidized bed models (Fig. 1b) with a wall separation distance of 15, 20, 30, and 50 mm were manufactured from Polylactic acid (PLA) by 3D-printing the walls. For all fluidized beds, compressed air was injected into the windbox with a diameter of 190 mm and a height of 150 mm. The air supply was controlled using a mass flow controller (F-203AV, Bronkhorst High-Tech B.V.) and homogenized with a distributor plate with a thickness of 10 mm with 6416 laser-cut holes with a diameter of 0.5 mm. The sections of the distributor plate that extended beyond the pseudo-2D fluidized bed were sealed from above with the 3D-printed wall and from below with tape. To determine the minimum fluidization velocity, the pressure drop of each fluidized bed model was measured with a pressure sensor using LabView (National Instruments, USA). All fluidized beds were filled up to a height of 210 mm with MCT oil-filled agar particles of Geldart-Group B with an average diameter of 1.02 ± 0.12 mm and a Sauter mean diameter of 1.019 mm. The density of the particles is 1.04 $\frac{g}{cm^3}$. Superficial gas velocities of 1, 1.2, 1.6, 1.8, and 2 times the minimum fluidization velocity (U_{mf}) were investigated, with the ratio determined from the measured minimum fluidization velocity of each particle-bed system.

Table 1
Experimental parameters for the local particle concentration and particle velocity MRI measurements.

Scan parameter	Local particle concentration		Particle velocity
Orientation:	horizontal	vertical	vertical
Field of view:	200 mm × 200 mm ($x \times z$)	205 mm × 326 mm ($x \times y$)	
Temporal resolution:	9.3 ms	9.3 ms	22.3 ms
Spatial resolution:	$3.125 \times 3 \times 10\,mm^3$ $x \times z \times y$	$3 \times 3 \times 10\,mm^3$ ($x \times y \times z$)	$3 \times 5 \times 10\,mm^3$
Flip angle:		15°	
Repetition time:	1.87 ms	8.7 ms	6.9 ms
Echo time:	0.85 ms	1.6 ms	2.27 ms
Velocity encoding:	–	–	1.5 m/s in x and y

2.2. Magnetic resonance imaging

The MRI measurements of this study were performed on a clinical MRI system (Philips Achieva, Philips Healthcare, The Netherlands) with a field strength of 3 T. Data were recorded with a custom-built 16-channel radio frequency receive coil, described in detail in Penn et al. (2017). Local particle concentration and velocity were acquired in a central vertical imaging plane. In the horizontal orientation, local particle concentration measurements were performed at a height of 150 mm above the distributor plate. Parallel imaging in combination with single-shot echo-planar imaging (EPI) (Stehling et al., 1991) and partial Fourier sampling was applied to increase the temporal resolution of particle distribution and velocity measurements to 9 ms and 22 ms, respectively. Particle velocity measurements were performed using MR phase-contrast velocimetry, achieved by applying bipolar motion-encoding gradients prior to the single-shot EPI readout. A total of three datasets were acquired, including velocity-encoded measurements in the x- and y-directions and a reference dataset obtained without applying bipolar velocity-encoding gradients to correct for background phase. Particle velocity data were acquired exclusively in x- and y-directions. The parameter of the MRI measurements are collected in Table 1.

2.3. Digital image analysis

A neural network was trained to segment MRI measurements into gas and particle phases. The neural network consists of a pretrained encoder and a decoder. On the encoder side, an EfficientNetV2-M (Tan and Le, 2021) was used with weights from (Wightman, 2019). On the decoder side, a single-channel U-Net (Ronneberger et al., 2015) was utilized. During preprocessing, the image intensities were normalized using reference scans from the fixed bed to homogenize the image intensity in all bed regions. All images were cropped to 96 × 64 pixels, which approximately corresponds to the area within the fluidized bed.

The U-Net on the decoder side was trained with a semi-automatic approach. A set of 300 images was manually segmented to train the initial version of the neural network. The initial network was used to automatically segment an additional 3000 images. These automatically segmented images were manually reviewed and corrected as needed. The final iteration of the neural network was trained using all 3300 segmented images. Training were conducted with a batch size of 32 for 10 epochs. During both training runs, image augmentation was applied to reduce overfitting. Augmentations include random image rotation, scaling, horizontal flipping, and minor contrast and brightness variations. In the supplementary material (Figs. S1 and S2), the segmentation of the neural network is compared with the previously used dynamic threshold method (Rennebaum et al., 2024, 2025).

2.4. Data evaluation

Segmented data were evaluated and analyzed using Python 3.11.0. From particle distribution measurements, the mean equivalent bubble diameter, d_{bub}, was determined as a function of the bed height (Figs. 3 and 5). The equivalent bubble diameter was determined from the detected area of a bubble, A_{bub} (Eq. (3)).

$$d_{bub} = \sqrt{\frac{4A_{bub}}{\pi}} \tag{3}$$

Bubbles with an area of less than $A_{bub} < 2\pi\Delta x\Delta y$ pixels, where Δx and Δy are the spatial resolution in the x-direction and the y-direction, respectively, were excluded from the evaluation.

The homogeneity of the radial bubble distribution was quantified using a ratio (Eq. (4)), ϵ, defined as the number of bubbles at a given radial distance weighted by their average area, divided by the average number of bubbles weighted by the average bubble area.

$$\epsilon = \frac{N_{bub}A_{bub}}{N_{bub,avg}A_{bub,avg}} \tag{4}$$

Bubble trajectories were determined on the basis of segmented frames using Kalman filtering. The trajectories were used to calculate the bubble rise velocity (Eq. (5)), v_{bub}. The bubble rise velocity was calculated from the change in position in y-direction divided by the time passed, t, between consecutive frames.

$$v_{bub} = \frac{y_{i,bub} - y_{i-1,bub}}{t_i - t_{i-1}} \tag{5}$$

Bubbles, which were detected in less than five frames, were excluded from the calculations. The bubble rise velocity was determined as a function of the equivalent bubble diameter as well as of the superficial gas velocity.

To evaluate the shape of the segmented bubbles (Eq. (6)), the aspect ratio, a_{ratio}, was determined from the maximum expansion in vertical orientation, d_v, and horizontal orientation, d_h (Fig. 8).

$$a_{ratio} = \frac{d_v}{d_h} \tag{6}$$

The bed expansion was calculated as the ratio of the fluidized bed height, h_0, at the superficial gas velocity to the bed height, h_{mf}, at the minimum fluidization velocity (Fig. 10). The height was determined by identifying the highest pixel connect to the bulk phase in each column. Horizontal MRI measurements were used to determine the optical accessibility of bubbles as a function of the equivalent bubble diameter. Bubbles with a height equal to the bed thickness, or up to one pixel smaller, were considered optically accessible. Different bed thicknesses and diameter ranges of bubbles were compared by a ratio of the number of optical accessible bubbles by the total number of bubbles.

The average in-plane velocity (Eq. (7)), $|v_{xy}|$, was calculated from particle velocity measurements with v_x as the measured velocity in x-direction and v_y as the measured velocity in y-direction.

$$|v_{xy}| = \frac{1}{N}\sum_{i=1}^{N}\sqrt{v_{x_i}^2 + v_{y_i}^2} \tag{7}$$

2.5. Optical measurements

Optical measurements were taken from two fluidized bed models with a bed thickness of 10 and 20 mm and a height of 500 mm made out of 10 mm thick antistatic PMMA plates. The width of both pseudo-2D fluidized beds were 200 mm. Air was distributed through a windbox with a height of 150 mm and a cross section of 80 and 250 mm. The air supply was provided by a mass flow controller (F-202AV/F-212AV, Bronkhorst High-Tech B.V.). The air entered through a 5 mm thick porous plate with a mean pore size of 20 µm. A backlight was used to illuminate the fluidized bed. Measurements were taken with a Chronos HD High Speed Camera (Kron Thechnologies, Canada) at a frame rate of 400 fps and a resolution of 1920 × 1080 (y-×x-direction). Superficial gas velocities of 1.6, 1.8, and 2 U_{mf} were investigated with two type of particles - glass beads and poppy seeds at a filling height of 210 mm. The glass beads have a Sauter mean diameter of 0.95 mm and a density of 2.54 $\frac{g}{cm^3}$, while the poppy seeds have a

Sauter mean diameter of 1.17 mm and a density of 1.16 $\frac{g}{cm^3}$. Data were segmented using a threshold-based approach. Compared to MRI data, optical methods provide higher spatial resolution, allowing for more reliable evaluations based on threshold-based segmentation. Segmented data were used to calculate the equivalent bubble diameter (Eq. (3)) and to confirm that the smallest equivalent bubble diameters were measured in the bed with a thickness of 20 mm, as observed in the MRI measurements.

3. Results and discussion

3.1. Minimum fluidization velocity

At the minimum fluidization velocity, the upward drag force exerted by the gas phase becomes equal to the gravitational force acting on the bed particles, initiating the transition from fixed to fluidized state (Anantharaman et al., 2018). The particles begin to suspend, making the minimum fluidization velocity one of the most essential parameters to describe fluidization processes. Extensive studies have been conducted to compare the minimum fluidization velocity within pseudo-2D and 3D fluidized beds (Sánchez-Delgado et al., 2011; Saxena and Vadivel, 1988). With decreasing bed thickness, wall effects intensify, resulting in an increase in the minimum fluidization velocity. In a pseudo-2D fluidized bed with a bed thickness of 15 mm used within the MRI measurements, fluidization begins at a gas velocity of 0.31 $\frac{m}{s}$, which is approximately 30 %, higher than the 3D bed velocity of 0.24 $\frac{m}{s}$. As the bed thickness increases, the minimum fluidization velocity gradually approaches the value of the 3D bed. For the thickness of the bed of 50 mm, the minimum fluidization velocity reached 0.26 $\frac{m}{s}$, which is within 8 % of the value measured in the 3D bed. The measured minimum fluidization velocities for all experimental setups are provided in the supplementary material (Tab. S1).

Fig. 2, shows the natural logarithm of the ratio between the minimum fluidization velocity in a pseudo-2D fluidized bed and that in comparable 3D systems, plotted against the bed thickness normalized by the particle diameter. In addition to the values measured in this study for fluidized bed used in the MRI measurements, the diagram is expanded with data (Sánchez-Delgado et al., 2011; Saxena and Vadivel, 1988; Saxena and Jadav, 1983) and models (Sánchez-Delgado et al., 2011; Saxena and Vadivel, 1988) from the literature.

The correlation of Saxena et al. was plotted for three different particle diameter and the model of Sánchez-Delgado et al. is plotted with the parameters of their work and those adapted to the specific bed conditions and particle system of this work. The correlations exhibit significant deviations from one another, which Sánchez-Delgado et al. attribute to two main factors: (a) electrostatic charge between particles and walls and (b) the particle shape (Sánchez-Delgado et al., 2011). Both electrostatically charged and nonspherical particles can increase the minimum fluidization velocity relative to that in a three-dimensional fluidized bed, resulting in data that align with the correlation of Saxena et al. The findings of this work provide additional support for this assumption. The data from the MRI setups, which showed electrostatic charge but were conducted with spherical particles, follow the correlation of Sánchez-Delgado et al. Using the parameters Sánchez-Delgado et al. suggest, the deviation from the measured minimum fluidization velocities is at most 15 % for the setups used in the MRI measurements. The authors recommend adjusting the parameters to match the specific system and particle configurations. With the optimized parameter, the deviation between the calculated and measured values is reduced to less than 5 %.

3.2. Spatial gas bubble distribution

Bubble parameters, such as the spatial gas bubble distribution, directly influence critical hydrodynamics such as flow patterns, solid mixing, and the interfacial area between the gas phase and the granular medium (Matsuura and Fan, 1984). Additionally, an uneven radial distribution of gas bubbles broadens the distribution of gas residence time and directly affects the efficiency of a process (Werther and Molerus, 1973). Therefore, to accurately predict the process efficiency of 3D fluidized beds based on pseudo-2D models, it is crucial that the bubble distribution exhibits similar patterns in both setups.

In Fig. 3, all segmented bubbles were collected from local particle concentration measurements. Near the distributor plate, the bubbles are evenly distributed throughout the width of all investigated beds. With increasing bed height, the bubble distribution within the 3D fluidized bed becomes increasingly centralized, with most bubbles rising at the center and few at the edges. In contrast, bubbles in pseudo-2D fluidized beds rise more frequently along the edges. Fig. 4 shows a quantitative comparison of spatial gas bubble distribution by plotting the ratio of the number of bubbles to the average number of bubbles weighted by the area of the bubble against the distance in x-direction from the center of the bed. For small distances, the 3D fluidized bed shows a elevated number of bubbles compared to thinner fluidized beds. The ratio decreases sharply near the edge and approaches close to zero, indicating that almost no bubbles rise at the edges of the bed. In contrast, pseudo-2D beds maintain higher values closer to one, reflecting a more uniform spatial gas bubble distribution. In the center of the bed, the bubble distribution is slightly more uniform compared to the 3D fluidized bed. For pseudo-2D fluidized beds, there appears to be no systematic dependence of the homogeneity of the bubble distribution on the thickness of the bed.

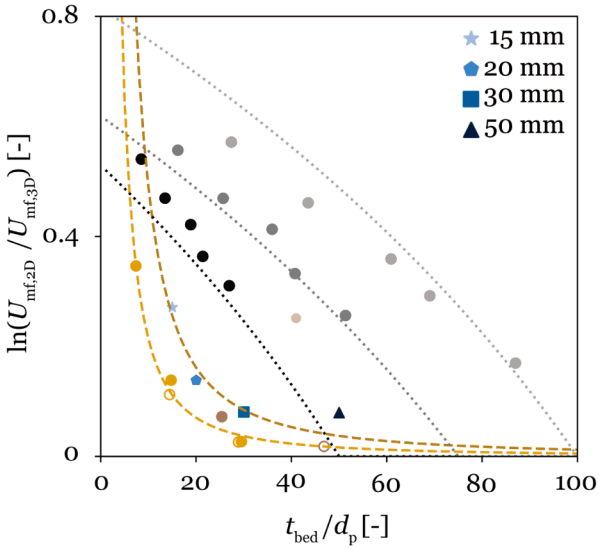

Fig. 2. Natural logarithm of the ratio between the minimum fluidization velocity in a 2D fluidized bed, $U_{mf,2D}$, and that in a comparable 3D systems $U_{mf,3D}$, over bed thickness normalized by the particle diameter. Data are compared to different correlations of Saxena and Vadivel (1988) (Eq. (1)) and Sánchez-Delgado et al. (2011) (Eq. (2)). The correlation of Saxena et al. is plotted for a particle diameter of -·- 0.73 mm, ····· 1.237 mm, and ····· 2.356 mm under the assumption that $U_{mf,2D}$ is the same as $U_{mf,3D}$ for t_{bed} is equal or greater than 100, 75, or 50 d_p, respectively. The model of Sánchez-Delgado et al. (2011) (Eq. (2)) is shown for --- parameters specified from their paper ($a = 8.5$ and $b = 1.6$) and --- parameters optimized ($a = 19.5$ and $b = 1.6$) for the measured minimum fluidization velocities taking into account the measured $U_{mf,3D}$ of 0.24 $\frac{m}{s}$. Blue data points were measured from this study, with the color tone indicating the bed thickness. The circlar marker indicate literture data of Saxena and Vadivel (1988) for particle diameter of ● 0.73, ● 1.237, and ● 2.356 mm, Sánchez-Delgado et al. for particle diameter of ○ 0.346 and ● 0.678 mm and a earlier study of Saxena and Jadav (1983) for particle diameter of ○ 0.427, ● 0.488, and ● 0.788 mm.

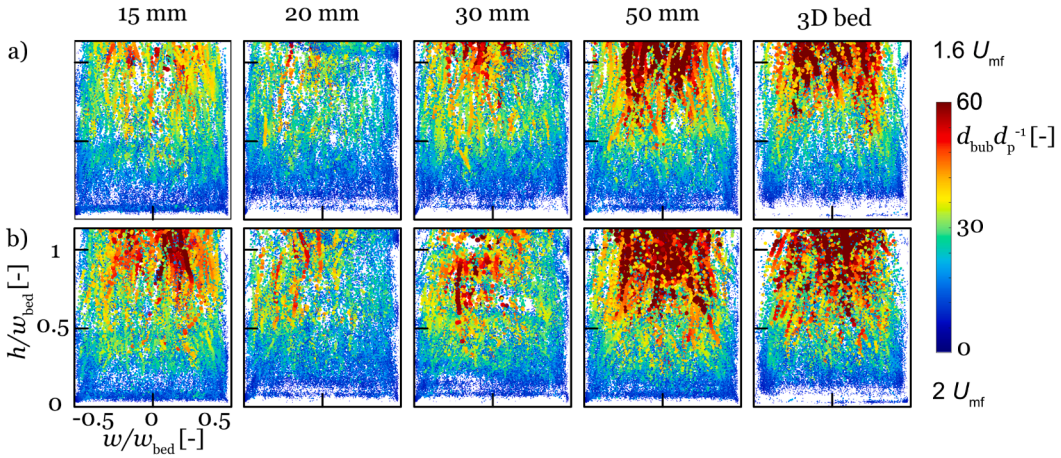

Fig. 3. MRI data used for extracting the spatial distribution of gas bubble centroids collected from 3000 frames in the central vertical imaging plane at superficial velocity of (a) 1.6 and (b) 2 U_{mf}. Bubbles are collected at their center of mass and the size and color of the circles depicted represent the size of the gas bubble, with small circles corresponding to small bubbles and large circles to large bubbles. From left to right, the measurements are sorted by bed thickness from 15 mm over 20, 30, and 50 mm to the 3D bed. Equivalent figures for the superficial gas velocities of 1.2 and 1.8 U_{mf} can be found in the supplementary material (Fig. S3).

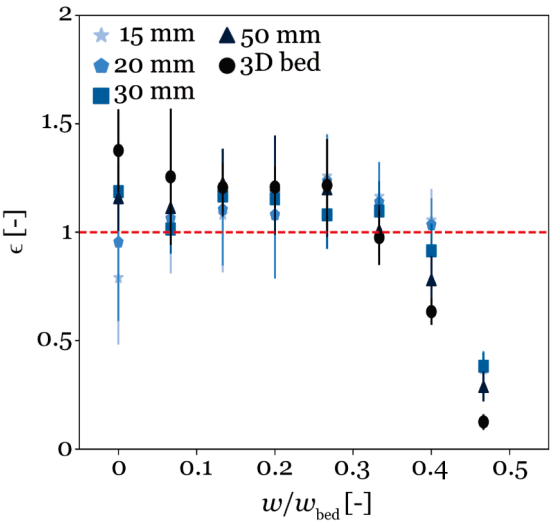

Fig. 4. The ratio of the number of bubbles to the average number of bubbles weighted by the bubble area for each dataset, denoted as ϵ, was plotted against the bed position at a superficial velocity of 2 U_{mf}. For each position, values from both sides of the fluidized bed were averaged. Bubbles located within one bed width (w_{bed}) above the distributor plate were taken into account. Values above one represent a higher bubble occurrence, whereas values below one indicate a lower occurrence compared to the average. Equivalent figures for the superficial gas velocities of 1.2, 1.6 and 1.8 U_{mf} can be found in the supplementary material (Figs. S4a and S5).

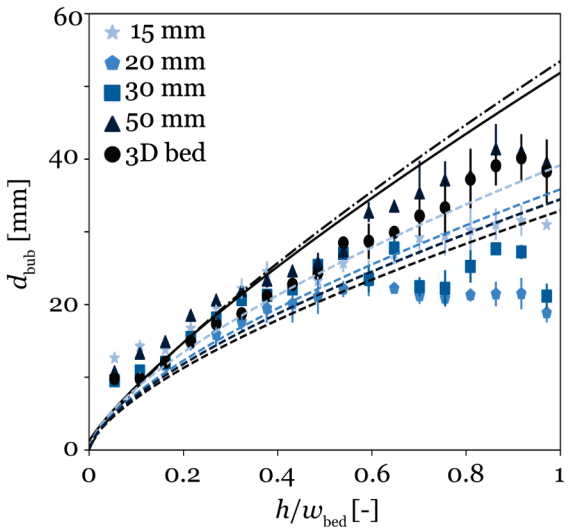

Fig. 5. Average equivalent bubble diameter over bed height normalized by the bed width for a superficial gas velocity of 2 U_{mf}. The measurements are compared to correlations of 3D fluidized beds of — Darton et al. (1977) and -·- Cai et al. (1994) and of pseudo-2D fluidized beds of Shen et al. (2004) for the different investigated bed thicknesses of – – – 15 mm, – – – 20 mm, – – – 30 mm, and – – – 50 mm. For the 3D correlations, the minimum fluidization velocity determined for the 3D fluidized bed was used, whereas for the correlation of Shen et al., the minimum fluidization velocity specific to each pseudo-2D particle-bed system was applied. The marker shape and the color denote the thickness of the fluidized bed. Equivalent figures for lower superficial gas velocities of 1.2, 1.6, and 1.8 U_{mf} can be found in the supplementary material (Figs. S4b and S6).

3.3. Size distribution and number of gas bubbles

The bubble size distribution within the different pseudo-2D beds and the 3D fluidized bed can be derived from the measurements shown in Fig. 3. In all investigated fluidized beds, the bubble size increases with distance from the distributor plate. The largest bubbles are observed at the center top of each setup, and the average bubble size increases with increasing superficial gas velocity. Previous studies, including those using MRI (Penn et al., 2019; Rennebaum et al., 2024), have shown the effect of bed height and superficial gas velocity on bubble size. In the lower half of the fluidized bed, the average bubble size does not show significant differences between the various configurations analyzed. In the upper half, smaller bubble sizes within the pseudo-2D fluidized beds with bed thicknesses between 15 mm and 30 mm can be observed. In the pseudo-2D fluidized bed with a larger bed thickness of 50 mm, the bubble size is comparable to that observed in the 3D fluidized bed. To allow a quantitative comparison of the average bubble size, in Fig. 5 the equivalent bubble diameter is plotted on the bed height normalized to the bed width. The measurements are compared with two correlations to predict the equivalent diameter over bed height for 3D fluidized beds and a correlation to determine the equivalent diameter in pseudo-2D fluidized bed for varying bed thicknesses.

The correlations for 3D fluidized beds are derived from the studies of Darton et al. (1977) and Cai et al. (1994). Both correlations include the difference between the superficial gas velocity and the minimum fluidization velocity. Additionally, the correlation devel-

oped by Darton et al. accounts for the open area of each orifice. The correlation to predict the equivalent diameter within pseudo-2D fluidized beds was introduced by Shen et al. (2004). The correlation estimates the equivalent bubble diameter based on the area of a single orifice in the distributor, the difference between the superficial gas velocity and the minimum fluidization velocity, and the bed thickness. Shen et al. introduced λ as a system-dependent constant which was adapted for this study to a value of 13.5, which minimized the sum of deviation from the measured values for all datasets at a superficial gas velocity of $2\,U_{mf}$. The measured data indicate that the equivalent bubble diameter increases with bed height in a similar manner for both the pseudo-2D fluidized bed with a bed thickness of 50 mm and the 3D fluidized bed, reaching a maximum equivalent bubble diameter of approximately 41 mm at the top of the bed. Both correlations for the equivalent bubble diameter in 3D fluidized beds agree well with the experimental data when small heights above the distributor plate are considered. For higher heights, the correlations overestimate the equivalent bubble diameter compared to the measured values. The overestimation of the equivalent bubble diameter for large bed heights is most pronounced at a superficial gas velocity of $2\,U_{mf}$. As the superficial gas velocity decreases, the agreement between the measured data and the correlations increases (Figs. S4b and S6). Overall, the 3D correlations are generally capable of accurately capturing the measured trends. While Shen et al.'s correlation, designed for estimating the equivalent bubble diameter in pseudo-2D fluidized beds, has proven effective in reproducing experimental data (Fu et al., 2024; Xu et al., 2025), it falls short of capturing the behavior consistently across all investigated bed thicknesses in this study. The measured data show that a reduction of the bed thickness to 20 mm decreases the measured equivalent bubble diameter to about 50 % of the value observed in the 3D bed, reaching approximately a maximum of 20 mm. At this point, the bubbles appear to reach an equilibrium between coalescence and splitting. In the upper half, the equivalent bubble diameter for the bed with a thickness of 30 mm fluctuates around an average of 25 mm, indicating a 40 % reduction in size compared to the 3D fluidized bed. The fluctuation observed in the 30 mm pseudo-2D fluidized bed measurement likely indicates data instability caused by a region of reduced coil sensitivity at the upper right edge, leading to false bubble detections. As this artefact lies within the evaluated range, it affects the results by decreasing the equivalent bubble diameter in this region and increasing the apparent number of bubbles. The measurements show that a decrease in bed thickness leads to a reduction in the average equivalent bubble diameter. Although the predicted values generally fall within the range of the experimental data, the model exhibits several shortcomings. In particular, the dependence on superficial gas velocity is overemphasized, as highlighted by comparisons at lower gas velocities (Figs. S4b and S6). The correlation proposed by Shen et al. tends to overpredict the equivalent bubble diameter at high superficial gas velocities and underpredict it at low velocities. Additionally, it fails to predict the plateau observed in pseudo-2D fluidized beds with small thicknesses at great bed heights, and it underestimates the influence of the bed thickness. Although the model predicts an increase in equivalent bubble diameter with increasing bed thickness, this effect is overstated. This is due to the variation in the minimum fluidization velocity with bed thickness (Fig. 2), which leads to a reduction in the predicted bubble diameter as bed thickness increases.

The measured data reveal a deviation from the general trend that narrower beds produce smaller bubbles in the narrowest pseudo-2D fluidized bed with a thickness of 15 mm. In this case, the reduction in bubble size is less pronounced compared to the thicker beds with thicknesses of 20 and 30 mm. The maximum equivalent bubble diameter in the 15 mm fluidized bed is 33 mm, which is a reduction of 20 % compared to the 3D fluidized bed. The observation of minimal equivalent bubble diameter within the pseudo-2D fluidized bed of 20 mm applies to all recorded datasets, including those for both particle density and particle velocity measurements. To demonstrate that this minimum is not due to a systematic error in the measurement method or limited to a specific particle system, optical measurements were performed on a pseudo-2D fluidized bed with bed thicknesses of 10 and 20 mm. The MRI and optical measurement data are qualitatively, rather than quantitatively, comparable, since particles with different properties were studied in similar but not identical fluidized beds. Fig. S8 in the supplementary material presents a comparison of the equivalent bubble diameters derived from optical and MRI measurements, highlighting and discussing the observed differences.

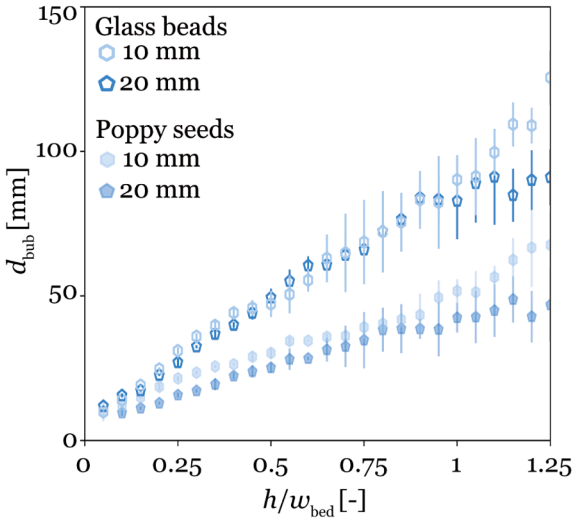

Fig. 6. Average equivalent bubble diameter over bed height normalized by the bed width for a superficial gas velocity of $2\,U_{mf}$. Data were obtained optically using a high-speed camera. The marker color specifies the thickness of the fluidized bed. Measurements for poppy seeds are shown as transparent, fully filled markers, while hollow markers correspond to measurements of glass beads. The glass beads exhibit higher sphericity, whereas the poppy seeds have a density similar to that of the MCT oil-filled particles used in this study. Optical measurements were conducted to allow for comparison with the MRI data. Bed thicknesses of 10 and 20 mm were examined. Equivalent figures for lower superficial gas velocities of 1.6 and $1.8\,U_{mf}$ can be found in the supplementary material (Fig. S7).

Fig. 6 shows the average equivalent bubble diameter obtained from these experiments plotted as a function of height within the fluidized bed. Consistent with the MRI experiments, the bed thickness does not affect the equivalent bubble diameter near the distributor plate. At a distance greater than 0.75 times the bed width from the distributor plate, differences can be observed. The larger bed thickness of 20 mm results in, on average, smaller equivalent bubble diameters for both particle types investigated — glass beads and poppy seeds. Additionally, glass beads, which have a higher density than poppy seeds, show larger equivalent bubble diameters. The optical measurements, similarly to the MRI measurements, show a minimum in equivalent bubble diameter for a bed thickness around 20 mm. One possible explanation is that as the bed thickness decreases, the available space for bubble formation becomes restricted, leading to less air being trapped in gas bubbles and more air remaining in the emulsion phase (Yang et al., 2017). The measurements indicate that bubble sizes in 3D beds can be more accurately resolved using either relatively narrow or thick pseudo-2D beds. Since thicker beds complicate optical resolution, the narrower configuration is generally preferred.

In Fig. 7, the average number of bubbles per frame is plotted over the bed height normalized by the bed diameter. After initial fluctuation, the number of bubbles continuously decreases with increasing bed heights for all investigated setups caused by bubble coalescence events, where two small bubbles grow to one larger bubble. Pseudo-2D fluidized beds with narrow bed thicknesses of 30 mm or less exhibit a higher number

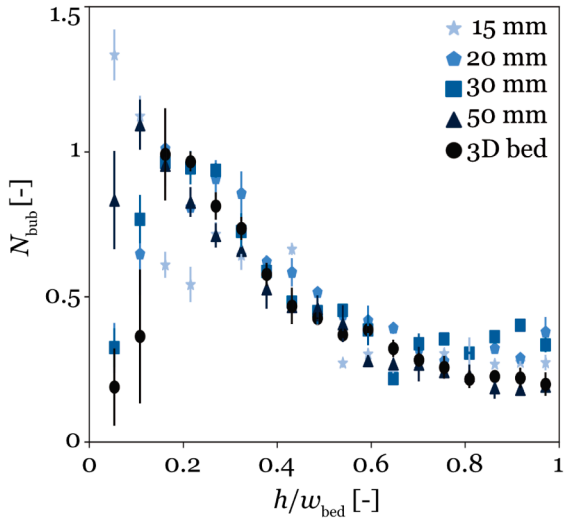

Fig. 7. Average number of bubbles per frame over bed height normalized by the bed width for a superficial gas velocity of $2\,U_{mf}$. The marker shape and the color denote the thickness of the fluidized bed. Equivalent figures for lower superficial gas velocities of 1.6 and $1.8\,U_{mf}$ can be found in the supplementary material (Fig. S9).

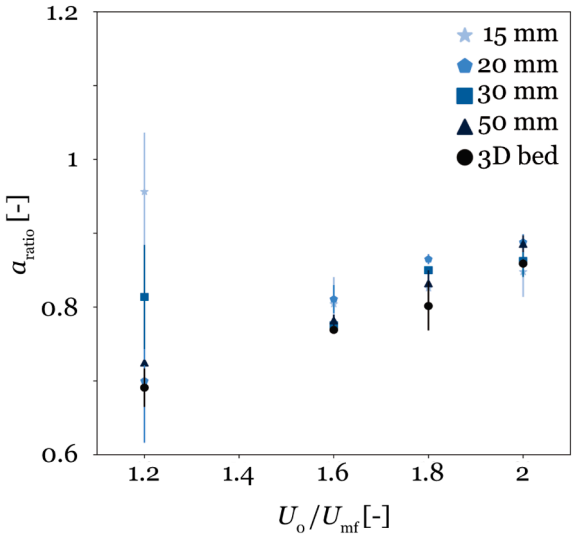

Fig. 8. Bubble aspect ratio averaged over the superficial gas velocity normalized by the minimum fluidization velocity of the specific particle-bed system. Low values of $a_{ratio} < 1$ correspond to oblate bubbles and values of $a_{ratio} > 1$ correspond to prolate bubbles. The average bubble aspect ratio is determined for all bubbles below a height of 190 mm above the distributor plate. The marker shape and the color denote the thickness of the fluidized bed.

of bubbles at higher bed heights. This aligns with the observation of a smaller equivalent bubble diameter at the same bed height within these setups, as shown in Fig. 5.

3.4. Bubble aspect ratio

In Fig. 8, the aspect ratio of a bubble, which is defined by a ratio of its maximum vertical extent to its maximum horizontal extent, is plotted on the superficial gas velocity. The aspect ratio indicates how much a bubble is deformed from a spherical shape (Yuan et al., 2024). Aspect ratios greater than one indicate bubbles with a prolate shape, while values less than one correspond to bubbles with an oblate shape. Fig. 8 shows that the aspect ratio increases with increasing superficial gas velocity. This dependency has already been presented by Salehi-Asl et al. (2018) within a pseudo-2D fluidized bed with a bed thickness of 15 mm. Under comparable conditions, the ratios reported in the study by Salehi-Asl et al. are greater than the values obtained in our study. However, the values remain within a similar range and vary between 0.8 and 1 over height for a superficial gas velocity of $1.5\,U_{mf}$. The comparison of the aspect ratio of 3D and pseudo-2D fluidized beds with varying bed thicknesses does not show any significant impact of the bed geometry on the bubble shape. Consequently, the bubble shape can be accurately approximated using the simplified pseudo-2D geometry.

3.5. Bubble rise velocity

In Fig. 9, the average bubble rise velocity is plotted over the superficial gas velocity. Gas bubbles rise faster for higher superficial gas velocities. This can be attributed to the larger average equivalent bubble diameter at higher superficial gas velocities and the tendency of larger bubbles to rise faster than smaller ones. For the 3D fluidized bed, the average bubble rise velocity indicates a linear growth with increasing superficial gas velocity, whereas in the pseudo-2D fluidized bed, the increase in the bubble rise velocity is saturated and slows down for large superficial gas velocity. The highest average bubble rise velocity is observed in the 3D fluidized bed, and it decreases with reduced bed thickness. The slower rise velocity in beds with smaller thicknesses can partially be explained by the detected reduction in the average equivalent bubble diameter (Figs. 3 and 5). However, there are two aspects that cannot be explained by the smaller bubbles in pseudo-2D compared

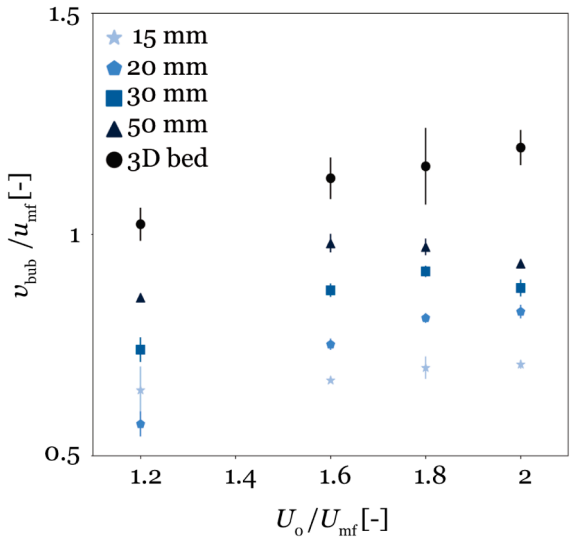

Fig. 9. Bubble rise velocity normalized by the minimum fluidization velocity was plotted over superficial gas velocity normalized by the minimum fluidization velocity of the specific particle-bed system. Bubbles which were detected and followed in less then five frames were not taken into account for the calculation. The marker shape and the color denote the thickness of the fluidized bed.

to 3D fluidized beds. Firstly, bubbles in a fluidized bed with a bed thickness of 50 mm rise slower than those in a 3D bed, although there are no significant differences in the equivalent bubble diameter between the two configurations. Secondly, bubbles in a fluidized bed with a thickness of 15 mm show the smallest rising velocities, even though the average equivalent bubble diameter was smaller for slightly larger bed thicknesses of 20 and 30 mm.

To determine whether the bed thickness impacts the bubbles' rise velocity within one equivalent diameter range, Fig. 10 shows the bubble rise velocity plotted against the equivalent bubble diameter. Each equivalent bubble diameter range comprises an interval of 10 mm. To establish a consistent database, data from all measured superficial gas

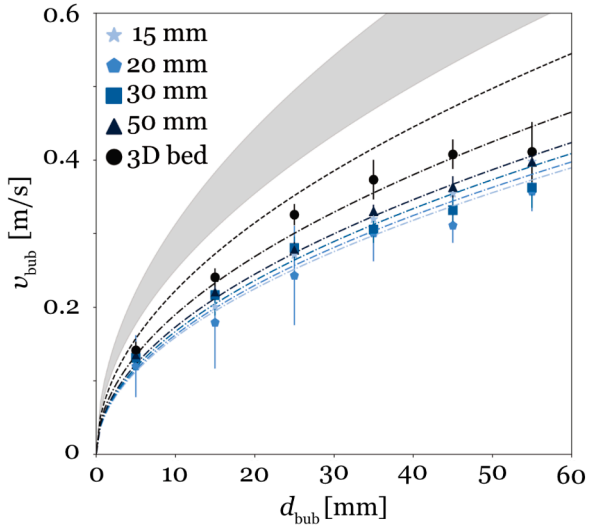

Fig. 10. Bubble rise velocity was plotted over equivalent bubble diameter ranges normalized by the particle diameter. Data were averaged over all measured superficial gas velocities. Bubbles which were detected and followed in less then five frames were not taken into account for the calculation. The marker shape and the color denote the thickness of the fluidized bed. Two different correlations to determine the bubble rise velocity of ····· Davidson et al. (1964) and Shen et al. (2004) were plotted. Proposed adaptation of the correlation (Eq. (8)) ····· for the 3D fluidized bed and the various bed thicknesses investigated in the pseudo-2D fluidized bed.

velocities were averaged. In all configurations, the bubble rise velocity increases with the equivalent bubble diameter. The smallest bubbles, with diameters ranging from 0 to 10 mm, exhibit similar rise velocities regardless of the bed thickness. For larger diameters, the bubble rise shows a dependency on bed thickness. Reducing the bed thickness leads to a slight decrease in the bubble rise velocity. The decrease in rise velocity can be attributed to the increased wall effect in thinner beds. Friction between the bubble and the wall can hinder and slow the bubble's rise.

In addition to the data obtained from the measurements, Fig. 10 includes two correlations (Shen et al., 2004; Davidson et al., 1964) that predict the bubble rise velocity based on their equivalent bubble diameter. Both models follow the same equation (Eq. (8)), where Φ is the bubble velocity coefficient.

$$v_{bub} = \Phi(g d_{bub})^{0.5} \tag{8}$$

Davidson et al. (1964) identified a value of 0.71 for Φ, while Shen et al. determined a higher value between 0.8 and 1 for Φ (Shen et al., 2004). The correlations capture the trend of the data but overestimate the bubble rise velocities for all diameters. The correlation proposed by Davidson et al. shows a closer agreement with the measured values than that of Shen et al. Although more accurate overall, Davidson et al.'s correlation still overestimates the velocity within the 3D fluidized bed by up to 21 %.

Furthermore, none of the existing correlations accounts for variations in bed thickness. To overcome this limitation, we extend the model of Davidson et al. (Eq. (8)) by incorporating a term that accounts for the reduced bed thickness in pseudo-2D fluidized beds.

$$v_{bub} = \Phi(g d_{bub})^{0.5} \left(\frac{t_{bed}}{w_{bed}}\right)^{\alpha} \tag{9}$$

In this approach, bed thickness is normalized by the bed width. The coefficient α which has be fitted to the specific particle system and experimental setup, was determined to be 0.07 and the value of Φ was determined as 0.61. These values were obtained by minimizing the quadratic deviation between the experimental data and the model predictions. Incorporating the dependency on bed thickness reduces the quadratic deviation by approximately 54 % compared to the model without this correction. The average deviation between the measured data and the correlation across all diameter ranges and bed thicknesses is below 6 %.

3.6. Bed expansion

The expansion of fluidized beds provides valuable information on the gas residence time within the bed, which in turn influences bubble dynamics and the mass transfer efficiency between the gas and solid phases (Llop et al., 2000). This is particularly important for processes that involve interfacial reactions, where an optimized residence time can significantly impact reaction rates and overall system performance. In Fig. 13, the expansion rate is plotted over the superficial gas velocity normalized by the minimum fluidization velocity. For all investigated fluidized beds, the expansion ratio increases with increasing superficial gas velocities. For a lower superficial gas velocity of $1.2\,U_{mf}$, the thickness and the geometry of the bed do not affect the expansion ratio, indicating a similar gas holdup for all investigated setups. At higher superficial gas velocities, the expansion ratio in the pseudo-2D fluidized system increases more than in the 3D system. At superficial gas velocities of 1.6 and $1.8\,U_{mf}$, all examined pseudo-2D fluidized beds, regardless of bed thickness, exhibit a similar expansion ratio. In contrast, at the highest superficial gas velocity of $2\,U_{mf}$, the expansion ratio becomes dependent on bed thickness and increases as the bed thickness decreases. This trend may be attributed to the 30 % higher minimum fluidization velocity observed in the thinnest pseudo-2D bed compared to the 3D bed (Fig. 2), leading to a higher gas volumetric flow rate per unit area and time. Furthermore, the residence time of the bubbles is extended in pseudo-2D fluidized beds leading to a higher expansion ratio, mainly due to their smaller average equivalent bubble diameter (Fig. 5) and the inherently slower rise velocity of bubbles of the same diameter range in three-dimensional fluidized beds (Fig. 10).

3.7. Optical accessibility

Optical accessibility of bubbles refers to how easily bubbles in a fluidized bed can be observed or imaged using optical methods. Bubbles that extend from the back to the front wall (Fig. 14a) are visible in optical measurements, whereas bubbles located in the center of the bed (Fig. 14b) may not be optically accessible. Horizontal MRI measurements were performed to evaluate how the optical accessibility depends on the bed thickness. Bubbles whose height was equal to the bed thickness, or up to one pixel smaller, were considered optically accessible. In Fig. 14c, the ratio of optically accessible bubbles to all detected bubbles is plotted as a function of bubble diameter. An increase in equivalent bubble diameter leads to higher optical accessibility. Smaller bubbles are detected optically less frequently, which may result in an overestimation of the equivalent bubble diameter in optical experiments. As expected, this effect becomes more pronounced with increasing bed thickness. The fraction of optically accessible bubbles across all diameter ranges decreases from approximately 58 % at a bed thickness of 15 mm to 49 %, 17 %, and 4 % at bed thicknesses of 20 mm, 30 mm and 50 mm, respectively.

3.8. Particle velocity

Measurements of particle velocities are necessary to understand the hydrodynamics of fluidized beds. Detecting high particle velocities is particularly important, as they can lead to increased particle attrition (Zhang et al., 2016). Therefore, when extrapolating the findings from pseudo-2D fluidized beds to 3D systems, it is essential to verify that comparable particle velocities are observed in both setups. Fig. 11a spatially resolves the average particle velocity averaged in x and y-direction for measurements at superficial gas velocities of $2\,U_{mf}$. In Fig. 11b and c, the velocities in y and x-direction are shown separately. Qualitatively, the particle velocities in pseudo-2D fluidized beds are similar to those observed in 3D configurations (Fig. 11a). Across all setups, the highest

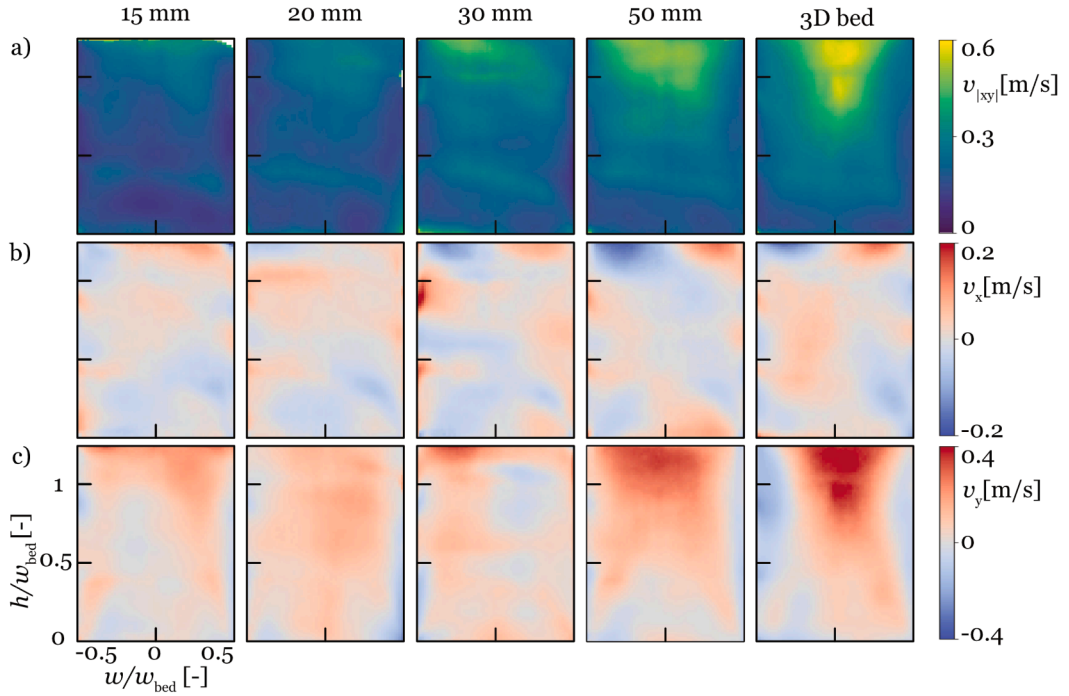

Fig. 11. Average particle velocities of (a) horizontal and vertical components, (b) horizontal components, and (c) vertical components for a superficial gas velocity of $2\,U_{mf}$. Horizontal and vertical components in (a) were calculated according to Eq. (5). From left to right, the measurements are sorted by bed thickness from 15 mm over 20, 30, and 50 mm to the 3D bed.

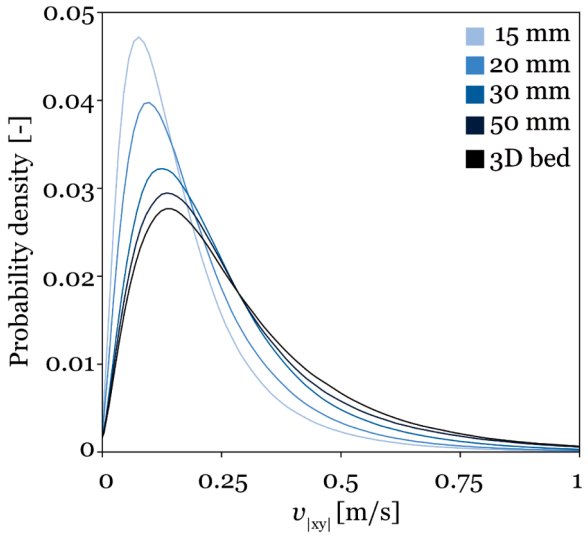

Fig. 12. Probability density of the average particle velocity of horizontal and vertical components for a superficial gas velocity of $2\,U_{mf}$ calculated according to Eq. 5. All velocity data points from a single dataset were visualized using a kernel density estimate (Python package: seaborn.kdeplot) with a bandwidth of 0.005.

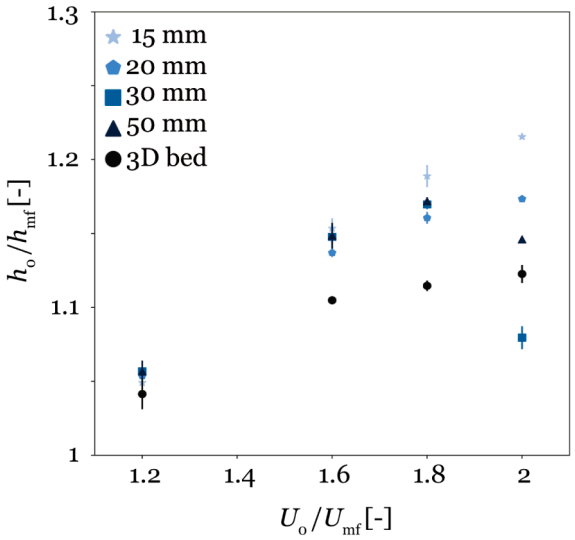

Fig. 13. Expansion ratio averaged over the superficial gas velocity normalized by the minimum fluidization velocity. The marker shape and the color denote the thickness of the fluidized bed.

average velocities occur at the central top region of the bed, while the lowest are found at the bottom. As anticipated, increasing the superficial gas velocity leads to higher average particle velocities. Fig. 11a shows that pseudo-2D fluidized beds typically decrease average particle velocities compared to those in 3D beds, with this discrepancy becoming more pronounced as bed thickness decreases. The lower velocities in pseudo-2D beds can be attributed to smaller bubbles and slower bubble rise velocities. Consequently, narrow pseudo-2D beds are not reliable for accurately approximating particle velocities in 3D systems. This limitation is particularly evident in PIV measurements, which record particle motion along the wall where friction and wall effects reduce the observed velocities (Li et al., 2012a). In contrast, MRI measurements capture velocities in the central vertical plane, where wall effects are reduced. Dividing the velocity data into horizontal (Fig. 11b) and vertical components (Fig. 11c) indicates that the particle velocity is dominated by the vertical component. The particles rise in the center and descend along the edges. In the 3D fluidized bed, the particles rise significantly faster than in pseudo-2D beds. For thinner beds with bed thicknesses of 15 and 30 mm, the vertical velocities deviate from the expected pattern (Patil et al., 2015; Tang et al., 2016). This deviation is likely caused by differences in magnetic susceptibility between air and wall materials, which affect the magnetic field near the walls. To alleviate this effect,

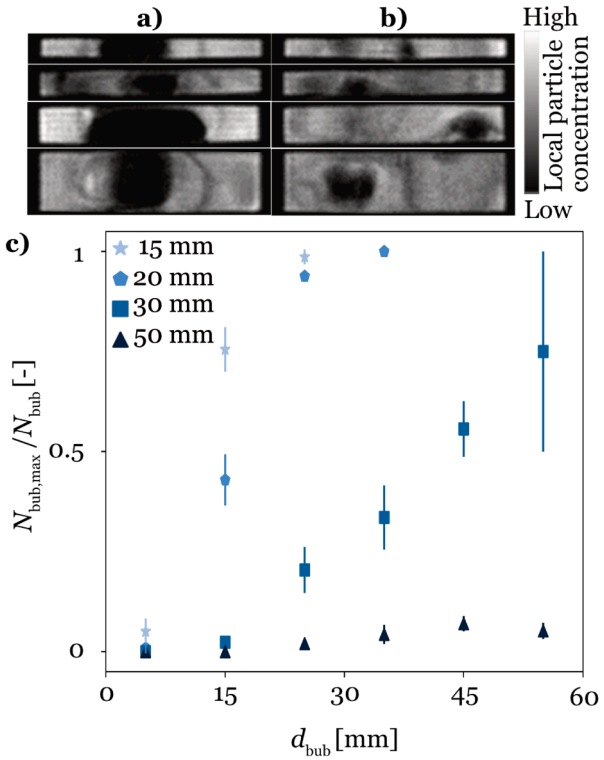

Fig. 14. Horizontally oriented MRI measurements for a superficial gas velocity of $2\,U_{mf}$ showing (a) bubbles extending from the back to the front wall and (b) bubbles that are interrupted. From top to bottom, the measurements are sorted by bed thickness from 15 mm over 20, and 30, to 50 mm. (c) Ratio of bubbles extending from the back to the front wall, allowing for at most one pixel of detected particles in between, plotted against the equivalent bubble diameter for a superficial gas velocity of $2\,U_{mf}$. The marker shape and the color denote the thickness of the fluidized bed.

complex susceptibility matching of all involved materials would be necessary in future studies. The horizontal velocities are of a similar magnitude in pseudo-2D and 3D fluidized beds. In the lower part of the bed, the horizontal motion tends to be directed toward the center, while in the upper part it is oriented more toward the edges. In the supplementary material (Fig. S11), the average particle velocities are additionally overlaid with streamlines indicating the direction of the particles.

In Fig. 12, the probability density of the particle velocity is shown to allow a more detailed comparison. As the bed thickness increases, the peak of the probability density shifts rightward, indicating a trend toward higher particle velocities. The distribution of particle velocities broadens with increasing bed thickness. As a result, there are fewer low particle velocities and more high particle velocities in the 3D bed compared to the pseudo-2D bed. In the 3D fluidized bed, 16 % of the particle velocities are below $0.1, \frac{m}{s}$. In contrast, this percentage more than doubles in the pseudo-2D fluidized bed with a bed thickness of 15 mm, rising to 36 %.

4. Conclusion

Pseudo-2D fluidized beds are an established method to simplify the investigation of hydrodynamics in fluidized beds. In this study, real-time MRI was used to evaluate the differences in hydrodynamics between pseudo-2D fluidized beds and 3D fluidized beds based on particle distribution and velocity measurements. The measurements show that the spatial gas bubble distribution over the bed width is more homogeneous within pseudo-2D fluidized beds, since more bubbles tend to rise at the edge of the bed. The average equivalent bubble diameter and the bubble rise velocity are smaller within pseudo-2D fluidized beds compared to 3D systems, but the shape of gas bubbles in 3D systems can be accurately predicted using pseudo-2D setups. At higher superficial gas velocities, pseudo-2D beds also exhibit a more pronounced bed expansion compared to a 3D bed. Additionally, particle velocities are lower in pseudo-2D setups. These differences become more pronounced as the bed thickness decreases. At a bed thickness of 50 mm, the pseudo-2D bed exhibits hydrodynamics similar to those of a 3D bed, with except for a lower bubble rise velocity. However, in most studies, the bed thickness is kept far below 50 mm, since achieving sufficient optical resolution becomes challenging. The MRI measurements in this work confirm this limitation by quantifying optical accessibility and demonstrating that, at larger bed thicknesses, many — especially smaller — bubbles are no longer visible. This finding supports the use of thinner beds in optical studies and highlights the necessity of tomographic methods for accurate characterization in 3D fluidized beds.

In the future, this work can be extended through a more comprehensive comparison with optical measurements of pseudo-2D fluidized beds. This includes analyses of particle velocities using PIV measurements, as well as the determination of bubble rise velocities and equivalent diameters at bed thicknesses similar to those investigated in this study. MRI measurements of the particle velocity can be extended along the z-direction to evaluate how the velocity is influenced in the dimension that is inaccessible to PIV measurements. If the magnetic susceptibility of the fluidized bed wall materials is matched to that of air, MRI measurements — particularly of particle velocity — could be significantly enhanced, allowing for the recording of an additional bed thickness of 10 mm. The adjusted magnetic susceptibility allows MRI measurements closer to the walls at higher bed thicknesses of 30 and 50 mm, making it possible to compare the central region with the areas near the edges.

Declaration of generative AI and AI-assisted technologies in the writing process

During the preparation of this work the authors used ChatGPT-4o in order to improve clarity and readability. After using this tool, the authors reviewed and edited the content as needed and take full responsibility for the content of the published article.

CRediT authorship contribution statement

Hannah S. Rennebaum: Writing – original draft, Visualization, Software, Investigation, Data curation; **Daniel L. Brummerloh:** Writing – review & editing, Software, Investigation; **Stefan Benders:** Writing – review & editing, Supervision, Investigation; **Alexander Penn:** Writing – review & editing, Supervision, Investigation, Funding acquisition.

Data availability

The neural network and training data will be made publicly available via the website of the institute. All other data will be made available on request.

Declaration of competing interest

The authors declare the following financial interests/personal relationships which may be considered as potential competing interests:

Alexander Penn reports financial support was provided by German Research Foundation. If there are other authors, they declare that they have no known competing financial interests or personal relationships that could have appeared to influence the work reported in this paper.

Acknowledgement

The authors thank Klaas P. Pruessmann from the University of Zurich and ETH Zurich for providing the opportunity to use their MRI facility for this work. The authors gratefully acknowledge the funding of this

project by Deutsche Forschungsgemeinschaft (DFG, German Research Council) under project number 471615686.

Supplementary material

Supplementary material associated with this article can be found in the online version at 10.1016/j.ces.2025.122977.

References

Anantharaman, A., Cocco, R.A., Chew, J.W., 2018. Evaluation of correlations for minimum fluidization velocity (u) in gas-solid fluidization. Powder Technol. 323, 454–485. https://doi.org/10.1016/j.powtec.2017.10.016

Boyce, C.M., Penn, A., Lehnert, M., Pruessmann, K.P., Müller, C.R., 2019a. Effect of liquid bridging on bubbles injected into a fluidized bed: a magnetic resonance imaging study. Powder Technol. 343, 813–820. https://doi.org/10.1016/j.powtec.2018.11.091

Boyce, C.M., Penn, A., Lehnert, M., Pruessmann, K.P., Müller, C.R., 2019b. Magnetic resonance imaging of single bubbles injected into incipiently fluidized beds. Chem. Eng. Sci. 200, 147–166. https://doi.org/10.1016/j.ces.2019.01.047

Cai, P., Schiavetti, M., de Michele, G., Grazzini, G.C., Miccio, M., 1994. Quantitative estimation of bubble size in PFBC. Powder Technol. 80 (2), 99–109. https://doi.org/10.1016/0032-5910(94)02834-6

Cano-Pleite, E., Shimizu, Y., Acosta-Iborra, A., Mawatari, Y., 2016. Effect of vertical vibration and particle size on the solids hold-up and mean bubble behavior in a pseudo-2D fluidized bed. Chem. Eng. J. 304, 384–398. https://doi.org/10.1016/j.cej.2016.06.095

Crowe, C.T., 2006. Multiphase Flow Handbook. Mechanical Engineering Series, CRC and Taylor & Francis, Boca Raton, FL. second ed.. https://permalink.obvsg.at/

Darton, R.C., LaNauze, R.D., Davidson, J.F., Harrison, D., 1977. Bubble growth due to coalescence in fluidised beds. Trans. Inst. Chem. Eng. 55 (4), 274–280.

Davidson, J.F., Harrison, D., Jackson, R., 1964. Fluidized particles. Chem. Eng. Sci. 19 (9), 701. https://doi.org/10.1016/0009-2509(64)85059-4

Errigo, M., Lettieri, P., Materazzi, M., 2023. X-ray imaging techniques for gas–solid fluidized beds: a technical review. Particuology. https://doi.org/10.1016/j.partic.2023.11.013

Fu, Y., He, X., Wang, S., Zhao, Y., Dong, L., Chen, Z., 2024. Study of bubble behavior in a gas–solid dense-phase fluidized bed based on deep learning. Fuel 357, 129889. https://doi.org/10.1016/j.fuel.2023.129889

Geldart, D., 1970. The size and frequency of bubbles in two- and three-dimensional gas-fluidised beds. Powder Technol. 4 (1), 41–55. https://doi.org/10.1016/0032-5910(70)80007-9

Geldart, D., Cranfield, R.R., 1972. The gas fluidisation of large particles. Chem. Eng. J. 3, 211–231. https://doi.org/10.1016/0300-9467(72)85024-X

Glicksman, L.R., McAndrews, G., 1985. The effect of bed width on the hydrodynamics of large particle fluidized beds. Powder Technol. 42 (2), 159–167. https://doi.org/10.1016/0032-5910(85)80049-8

Guo, Q., Zhang, Y., Padash, A., Xi, K., Kovar, T.M., Boyce, C.M., 2021. Dynamically structured bubbling in vibrated gas-fluidized granular materials. Proc. Natl. Acad. Sci. USA 118 (35). https://doi.org/10.1073/pnas.2108647118

Hagemeier, T., Roloff, C., Bück, A., Tsotsas, E., 2015. Estimation of particle dynamics in 2-d fluidized beds using particle tracking velocimetry. Particuology 22, 39–51. https://doi.org/10.1016/j.partic.2014.08.004

He, C., Bi, X.T., Grace, J.R., 2015. Monitoring electrostatics and hydrodynamics in gas–solid bubbling fluidized beds using novel electrostatic probes. Ind. Eng. Chem. Res. 54 (33), 8333–8343. https://doi.org/10.1021/acs.iecr.5b01512

Hernández-Jiménez, F., Sánchez-Delgado, S., Gómez-García, A., Acosta-Iborra, A., 2011. Comparison between two-fluid model simulations and particle image analysis & velocimetry (PIV) results for a two-dimensional gas–solid fluidized bed. Chem. Eng. Sci. 66 (17), 3753–3772. https://doi.org/10.1016/j.ces.2011.04.026

Hernández-Jiménez, F., Sánchez-Prieto, J., Soria-Verdugo, A., Acosta-Iborra, A., 2013. Experimental quantification of the particle–wall frictional forces in pseudo-2D gas fluidised beds. Chem. Eng. Sci. 102, 257–267. https://doi.org/10.1016/j.ces.2013.08.020

de Jong, J.F., van Sint Annaland, M., Kuipers, J.A.M., 2013. Experimental study on the hydrodynamic effects of gas permeation through horizontal membrane tubes in fluidized beds. Powder Technol. 241, 74–84. https://doi.org/10.1016/j.powtec.2013.03.014

Laverman, J.A., Roghair, I., van Annaland, M.S., Kuipers, H., 2008. Investigation into the hydrodynamics of gas–solid fluidized beds using particle image velocimetry coupled with digital image analysis. Can. J. Chem. Eng. 86 (3), 523–535. https://doi.org/10.1002/cjce.20054

Li, T., Gopalakrishnan, P., Garg, R., Shahnam, M., 2012a. Cfd–dem study of effect of bed thickness for bubbling fluidized beds. Particuology 10 (5), 532–541. https://doi.org/10.1016/j.partic.2012.02.006

Li, X., Yang, C., Yang, S., Li, G., 2012b. Fiber-optical sensors: basics and applications in multiphase reactors. Sensors 12 (9), 12519–12544. https://doi.org/10.3390/s120912519

Llop, M.F., Casal, J., Arnaldos, J., 2000. Expansion of gas–solid fluidized beds at pressure and high temperature. Powder Technol. 107 (3), 212–225. https://doi.org/10.1016/S0032-5910(99)00188-6

Mahajan, V.V., Padding, J.T., Nijssen, T. M.J., Buist, K.A., Kuipers, J.A.M., 2018. Non-spherical particles in a pseudo-2D fluidized bed: experimental study. AIChE J. 64 (5), 1573–1590. https://doi.org/10.1002/aic.16078

Matsuura, A., Fan, L.-S., 1984. Distribution of bubble properties in a gas–liquid–solid fluidized bed. AIChE J. 30 (6), 894–903. https://doi.org/10.1002/aic.690300604

Maurer, S., Wagner, E.C., Schildhauer, T.J., van Ommen, J.R., Biollaz, S. M.A., Mudde, R.F., 2015. X-ray measurements on the influence of optical probes on gas–solid fluidized beds. Int. J. Multiph. Flow 74, 143–147. https://doi.org/10.1016/j.ijmultiphaseflow.2015.04.002

Patil, A.V., Peters, E.A.J.F., Sutkar, V.S., Deen, N.G., Kuipers, J.A.M., 2015. A study of heat transfer in fluidized beds using an integrated DIA/PIV/IR technique. Chem. Eng. J. 259, 90–106. https://doi.org/10.1016/j.cej.2014.07.107

Penn, A., Boyce, C.M., Conzelmann, N., Bezinge, G., Pruessmann, K.P., Müller, C.R., 2019. Real-time magnetic resonance imaging of fluidized beds with internals. Chem. Eng. Sci. 198, 117–123. https://doi.org/10.1016/j.ces.2018.12.041

Penn, A., Boyce, C.M., Kovar, T., Tsuji, T., Pruessmann, K.P., Müller, C.R., 2018. Real-time magnetic resonance imaging of bubble behavior and particle velocity in fluidized beds. Ind. Eng. Chem. Res. 57 (29), 9674–9682. https://doi.org/10.1021/acs.iecr.8b00932

Penn, A., Tsuji, T., Brunner, D.O., Boyce, C.M., Pruessmann, K.P., Müller, C.R., 2017. Real-time probing of granular dynamics with magnetic resonance. Sci. Adv. 3 (9), e1701879. https://doi.org/10.1126/sciadv.1701879

Ramos Caicedo, G., Garcıéa Ruiz, M., Prieto Marqués, J.J., Guardiola Soler, J., 2002. Minimum fluidization velocities for gas–solid 2D beds. Chem. Eng. Process. 41 (9), 761–764. https://doi.org/10.1016/S0255-2701(02)00005-3

Rennebaum, H.S., Brummerloh, D.L., Benders, S., Penn, A., 2024. The effect of baffles on the hydrodynamics of a gas-solid fluidized bed studied using real-time magnetic resonance imaging. Powder Technol. 432, 119114. https://doi.org/10.1016/j.powtec.2023.119114

Rennebaum, H.S., Müller, C.R., Penn, A., 2025. Vertical tubes in bubbling fluidized beds: a magnetic resonance imaging study of particle and bubble behavior. Powder Technol. 457, 120870. https://doi.org/10.1016/j.powtec.2025.120870

Ronneberger, O., Fischer, P., Brox, T., 2015. U-net: Convolutional networks for biomedical image segmentation. https://doi.org/10.48550/arXiv.1505.04597

Rüdisüli, M., Schildhauer, T.J., Biollaz, S. M.A., van Ruud Ommen, J., 2012. Bubble characterization in a fluidized bed by means of optical probes. Int. J. Multiph. Flow 41, 56–67. https://doi.org/10.1016/j.ijmultiphaseflow.2012.01.001

Salehi-Asl, M., Azhgan, S., Movahedirad, S., 2018. Some general aspects of a gas-solid fluidized bed using digital image analysis. Korean J. Chem. Eng. 35 (2), 613–620. https://doi.org/10.1007/s11814-017-0291-y

Sánchez-Delgado, S., Almendros-Ibáñez, J.A., García-Hernando, N., Santana, D., 2011. On the minimum fluidization velocity in 2D fluidized beds. Powder Technol. 207 (1–3), 145–153. https://doi.org/10.1016/j.powtec.2010.10.020

Saxena, S.C., Jadav, S., 1983. A two-dimensional gas fluidized bed for hydrodynamic and elutriation studies. Powder Technol. 36 (1), 61–70. https://doi.org/10.1016/0032-5910(83)80009-6

Saxena, S.C., Vadivel, R., 1988. Wall effects in gas-fluidized beds at incipient fluidization. Chem. Eng. J. 39 (2), 133–137. https://doi.org/10.1016/0300-9467(88)80104-7

Shen, L., Johnsson, F., Leckner, B., 2004. Digital image analysis of hydrodynamics two-dimensional bubbling fluidized beds. Chem. Eng. Sci. 59 (13), 2607–2617. https://doi.org/10.1016/j.ces.2004.01.063

Stehling, M.K., Turner, R., Mansfield, P., 1991. Echo-planar imaging: magnetic resonance imaging in a fraction of a second. Science (New York, N.Y.) 254 (5028), 43–50. https://doi.org/10.1126/science.1925560

Tan, M., Le, Q.V., 2021. Efficientnetv2: smaller models and faster training. https://doi.org/10.48550/arXiv.2104.00298

Tang, Y., Lau, Y.M., Deen, N.G., Peters, E.A.J.F., Kuipers, J.A.M., et al., 2016. Direct numerical simulations and experiments of a pseudo-2D gas-fluidized bed. Chem. Eng. Sci. 143, 166–180. https://doi.org/10.1016/j.ces.2015.12.026

Taofeeq, H., Aradhya, S., Shao, J., Al-Dahhan, M., 2018. Advance optical fiber probe for simultaneous measurements of solids holdup and particles velocity using simple calibration methods for gas-solid fluidization systems. Flow Meas. Instrum. 63, 18–32. https://doi.org/10.1016/j.flowmeasinst.2018.07.001

Varghese, M.M., Mangadoddy, N., Vakamalla, T.R., 2021. Experimental study of gas-solid fluidized bed hydrodynamics using optical fiber probe. In: Prabu, T., Viswanathan, P., Agrawal, A., Banerjee, J. (Eds.), Fluid Mechanics and Fluid Power. Springer Singapore, Singapore. Lecture Notes in Mechanical Engineering, pp. 787–794. https://doi.org/10.1007/978-981-16-0698-4{_}87

Werther, J., Molerus, O., 1973. The local structure of gas fluidized beds—II. The spatial distribution of bubbles. Int. J. Multiph. Flow 1 (1), 123–138. https://doi.org/10.1016/0301-9322(73)90008-6

Wiesendorf, V., Werther, J., 2000. Capacitance probes for solids volume concentration and velocity measurements in industrial fluidized bed reactors. Powder Technol. 110 (1–2), 143–157. https://doi.org/10.1016/S0032-5910(99)00276-4

Wightman, R., 2019. Pytorch image models. https://doi.org/10.5281/zenodo.4414861

Winkler, F., 1926. Verfahren zum herstellen von wassergas.

Xu, X., Zhang, G., Chen, Z., Zhang, Z., Dong, L., 2025. Experimental investigation on the bubble characteristics in a gas-solid sound-assisted separation fluidized bed. Chem. Eng. Res. Des. 214, 1–17. https://doi.org/10.1016/j.cherd.2024.12.023

Yang, L., Padding, J.T., Buist, K.A., Kuipers, J.A.M., 2017. Three-dimensional fluidized beds with rough spheres: validation of a two fluid model by magnetic particle tracking and discrete particle simulations. Chem. Eng. Sci. 174, 238–258. https://doi.org/10.1016/j.ces.2017.09.014

Yuan, Z., Feng, Y., Huang, Z., Ma, S., Yang, H., Yue, G., 2024. Effects of particle size on bubble dynamic behaviors in a quasi-two-dimensional gas-solid fluidized bed. Powder Technol. 436, 119451. https://doi.org/10.1016/j.powtec.2024.119451

Zhang, H., Degrève, J., Baeyens, J., Wu, S.-Y., 2016. Powder attrition in gas fluidized beds. Powder Technol. 287, 1–11. https://doi.org/10.1016/j.powtec.2015.08.052

Zhu, X., Liu, Y., Jiang, X., Wang, H., Wang, Z., Bai, Z., Ocone, R., 2023. Effects of pressure and particle size on bubble behaviors in a pseudo 2D pressured fluidized bed with geldart a/b, b and d particles. Chem. Eng. J. 470, 143904. https://doi.org/10.1016/j.cej.2023.143904